

Composition-, Size-, and Surface Functionalization-Dependent Optical Properties of Lead Bromide Perovskite Nanocrystals

Palvasha Ijaz, Muhammad Imran, Márcio M. Soares, Hélio C. N. Tolentino, Beatriz Martín-García, Cinzia Giannini, Iwan Moreels, Liberato Manna,* and Roman Krahne*

Cite This: *J. Phys. Chem. Lett.* 2020, 11, 2079–2085

Read Online

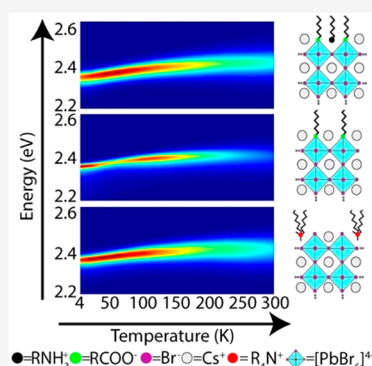
ACCESS |

Metrics & More

Article Recommendations

Supporting Information

ABSTRACT: The photoluminescence (PL), color purity, and stability of lead halide perovskite nanocrystals depend critically on surface passivation. We present a study on the temperature-dependent PL and PL decay dynamics of lead bromide perovskite nanocrystals characterized by different types of A cations, surface ligands, and nanocrystal sizes. Throughout, we observe a single emission peak from cryogenic to ambient temperature. The PL decay dynamics are dominated by surface passivation, and a postsynthesis ligand exchange with a quaternary ammonium bromide (QAB) results in more stable passivation over a larger temperature range. The PL intensity is highest from 50 to 250 K, which indicates that ligand binding competes with the thermal energy at ambient temperature. Despite the favorable PL dynamics of nanocrystals passivated with QAB ligands (monoexponential PL decay over a large temperature range, increased PL intensity and stability), surface passivation still needs to be improved to achieve maximum emission intensity in nanocrystal films.



The optical properties of colloidal semiconductor nanocrystals (NCs) have been widely investigated in the past three decades. It has been well established that the composition and nature of the NC surface strongly influence their optical properties.^{1–3} Recently, lead halide perovskite NCs (LHP NCs), with an APbX_3 composition (with A being a monovalent cation and X being either Cl, Br, or I), have emerged as a promising material due to their ease of preparation, broadly tunable band gap, high photoluminescence quantum yield (PLQY), and excellent color purity.^{4–8} This remarkable set of properties makes them ideal candidates for light emission technologies, such as light-emitting diodes, lasers, and single-photon emitters.^{9–11}

Significant progress has been made on the synthesis of LHP NCs, especially with regard to size, shape, and composition control and by tailoring surface passivation through direct synthesis or by postsynthesis ligand exchange.⁴ Advancements in the synthesis of LHP NCs not only have paved the way to study shape- and composition-dependent optical properties but also have offered a great opportunity to elucidate the effects of surface functionalization. PL spectroscopy at cryogenic temperatures has been used to investigate the temperature-dependent excitonic properties of traditional semiconductors and recently of LHP NCs.^{12–14} In this respect, there has been some disagreement in the literature about whether LHP NCs undergo temperature-induced phase transitions from room temperature to cryogenic temperatures, whether the emission at cryogenic temperatures consists of a single peak or multiple peaks,^{15–20} and, in the latter case, on the exact origin of these multiple peaks.

From a surface chemistry point of view, the first generation of LHP NCs was typically prepared by using primary alkyl amines and alkyl carboxylates as surfactants, and it was established that both ligands are present on the surface of the NCs, bound as Cs carboxylate/alkyl ammonium bromide ligand pairs (henceforth termed “mixed ligand capped NCs”).^{21–25} Substantial advances in colloidal synthesis and postsynthesis treatments over the past few years have provided the opportunity to prepare LHP NCs with diverse surface coatings, leading to tailored properties, such as improved colloidal stability and near-unity PLQY.^{26–29} However, investigations based on optical spectroscopy were mainly limited to the first generation of NCs, i.e., those characterized by a mixed ligand surface passivation. Considering the recent developments in the synthesis of monodisperse NCs and in surface functionalization, a temperature-dependent optical spectroscopy study of trap-free, near-unity PLQY NCs should provide further insights into the effect of size, composition, and surface passivation on their excitonic properties.

In this work, we study the photoluminescence properties of APbBr_3 ($A = \text{Cs}, \text{MA}, \text{or FA}$) NCs with respect to temperature, NC size, and surface passivating ligands and observe the following. (i) All samples manifest a single narrow emission

Received: January 27, 2020

Accepted: February 23, 2020

Published: February 23, 2020

peak at room and cryogenic temperatures. Because our temperature-dependent XRD study excludes phase transitions, we conclude that the possible observation of multiple emission peaks at low temperatures (as was reported in the literature^{16–20}) is related to polydispersity of the samples. (ii) The PL intensity is strongest in an intermediate temperature regime that spans from ~ 50 to 250 K, while the PL lifetime decreases with a decrease in temperature in the range from room temperature (RT) to ~ 50 K. PL and PL lifetimes below 50 K become strongly surface dependent, and this may be ascribed to the possible phase transition in the organic capping layer, as previously reported for CdSe NCs.^{30,31} This behavior indicates that ligand binding can still be improved significantly to provide the most efficient surface passivation at temperatures that are relevant for optoelectronic applications, i.e., at and above RT. (iii) The temperature-induced PL red-shift¹⁴ is more dominant in larger NCs than in smaller NCs. However, we do not observe any significant impact of NC size on the spectral shape of the emission or on the lifetime dynamics. (iv) Surface passivation affects the temperature dependence of the PL and the PL lifetime. Here, exchanging the ligands from Cs oleate with quarternary ammonium bromide (QAB) ones (didodecyldimethylammonium bromide) results in a higher PL intensity over an extended temperature range (from 20 to 280 K). Also, the PL decay dynamics are notably different for QAB ligands, showing a monoexponential decay over a large temperature range, while Cs oleate and mixed ligand capped NCs develop a biexponential decay at or shortly below room temperature due to a fast nonradiative decay component. This behavior points to less effective ligand passivation at lower temperatures, which we ascribe to the reduced dynamics of ligand binding at the NC surface.

The APbBr₃ perovskite NCs were synthesized following our benzoyl halide-based procedure, as reported previously³² (see Experimental Section in the Supporting Information for details). They were prepared using oleylamine and oleic acid as surfactants; hence, they have a mixed ligand passivation (Cs oleate and oleylammonium bromide). Transmission electron microscopy (TEM) images of CsPbBr₃, MAPbBr₃, and FAPbBr₃ are shown in panels a–c, respectively, of Figure 1. The images show that the NCs are nearly monodisperse, with roughly cubic shapes in all cases. Typical ultraviolet–visible (UV–vis) optical absorption and PL spectra, measured in toluene dispersions, are reported in Figure 1d, displaying a single emission peak that is red-shifted from the absorption edge.

For the temperature-dependent spectroscopic study, NC films were prepared on sapphire substrates by drop-casting from the colloidal dispersions. We first focus on the samples that are characterized by different A cations and passivated by a mixed ligands. The films were cooled to 4 K, and the temperature was increased stepwise from 4 to 300 K to acquire the PL spectra and PL lifetime decay. The representative PL spectra recorded at 4 and 300 K are shown in Figure 2a, whereas the complete range of PL spectra acquired at various temperatures is shown in Figures S1–S3. At 4 K, the PL peak energy is red-shifted by 70, 110, and 80 meV for Cs-, MA-, and FA-based perovskite NCs with respect to the corresponding spectra at RT. Such a red-shift with a decrease in temperature is commonly observed in lead halide perovskites and has been attributed to a temperature dependence of the overlap between the Pb 6s and Br 4p orbitals, leading to a decrease in the band

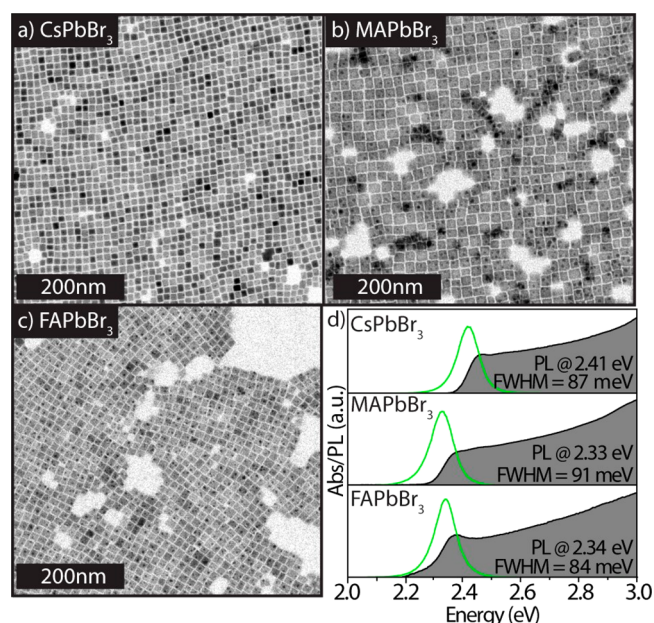


Figure 1. APbBr₃ NCs prepared by using oleylamine and oleic acid as surfactants, hence having a mixed ligand passivation of Cs oleate and oleylammonium bromide (A = Cs, MA, or FA). TEM images of (a) CsPbBr₃, (b) MAPbBr₃, and (c) FAPbBr₃ NCs. The mean values of the edge lengths of the NCs in panels a–c are 9.2 ± 0.8 , 17.3 ± 1.6 , and 12.9 ± 1.4 nm, respectively. (d) Absorbance and PL spectra of the corresponding NC samples in toluene dispersions.

gap with a decrease in temperature,^{14,33–35} and recently was found to be dependent on size.³⁶ The MAPbBr₃ NCs manifest the strongest temperature-related red-shift in PL peak energy, which can be ascribed to their larger NC size (see also the size dependence discussion below). The quantitative analysis showing the trends in temperature-dependent PL spectra, the PL peak energy and line width, and the average PL decay times are reported in Figures S4 and S5 for the three NC samples. Fitting the temperature dependence of the PL line width indicates that homogeneous broadening is dominated by coupling to LO phonons,³⁷ where we obtain LO phonon energies in the range of 10–40 meV (see Figure S6 and Table S4 and the related discussion). PL intensity versus temperature is plotted in Figure 2b. For all three samples, the PL intensity is highest at intermediate temperatures (around 50–250 K) and decreases toward 4 and 300 K. The PL decay traces recorded at different temperatures are reported in Figure 2c, and their average PL lifetimes (including fitting parameters) are reported in Tables S1–S3. At room temperature, the PL decay is almost monoexponential, and then, with a decrease in temperature, it develops a multiexponential trace with fast and slow components. At <70 K, the drop in PL intensity indicates that the nonradiative rates gain weight.

The PL emission properties of a film of perovskite NCs are expected to depend on the size dispersion of the sample and its surface chemistry. To investigate the impact of the surface chemistry, we decided to focus on the NC sample with Cs as the A site cation (CsPbBr₃) and prepared two additional samples, characterized by two types of surface coatings that are different from the mixed ligands discussed above (Figure 3a–c). These were Cs oleate-coated NCs in one case and QAB-coated NCs in the other (see Figure 3). Cs oleate-coated NCs were prepared by performing the synthesis using a secondary amine instead of oleylamine. The procedure is discussed in a

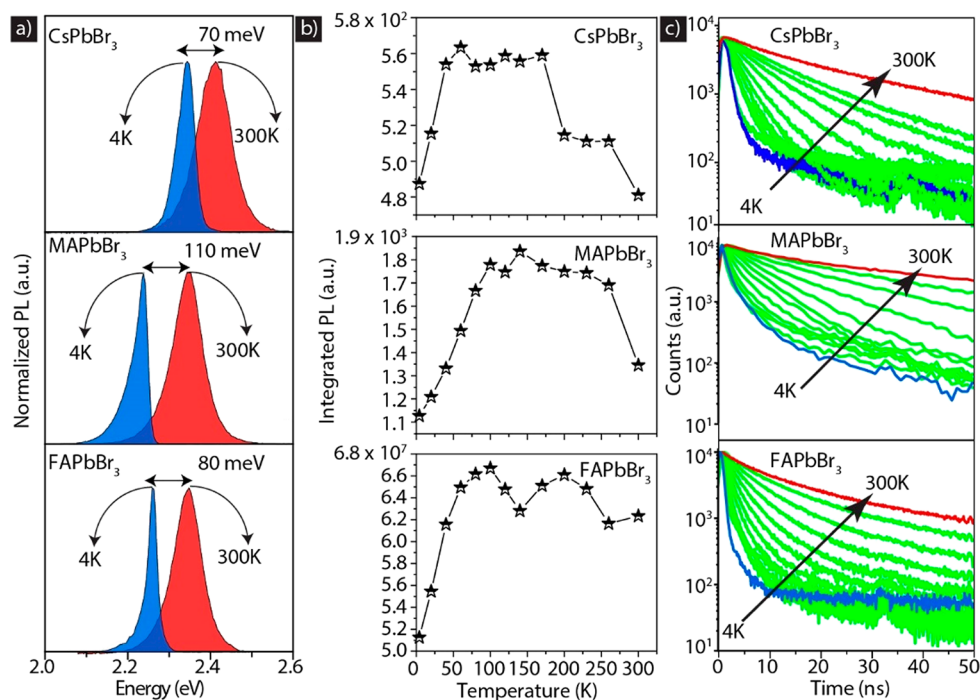


Figure 2. Photoluminescence characteristics of mixed ligand capped CsPbBr₃, MAPbBr₃, and FAPbBr₃ NC films. (a) Representative PL spectra recorded at 4 and 300 K. (b and c) Integrated PL intensity and PL decay traces, respectively, at different temperatures.

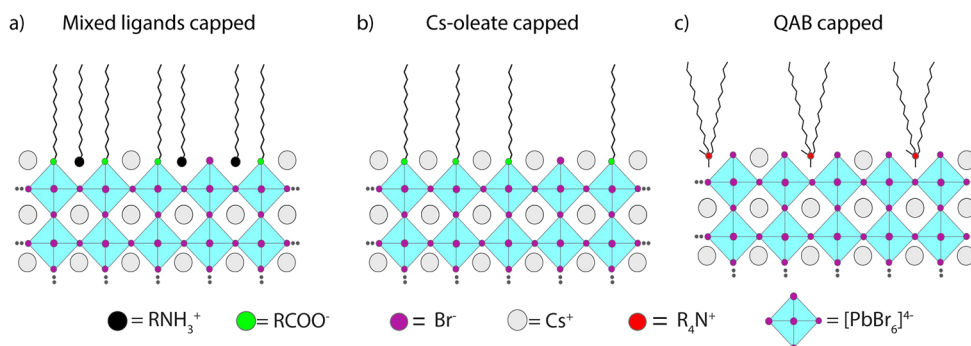


Figure 3. Schematic illustration of CsPbBr₃ NCs with different surface passivation: (a) mixed ligands (Cs oleate and oleylammonium bromide), (b) Cs oleate, and (c) QAB (didodecyldimethylammonium bromide).

previous work of ours, which demonstrated that the secondary amines cannot bind to the surface of NCs,³⁸ leaving only Cs oleate as the surface coating agent. This synthesis delivers NCs with narrow size distributions and prevents the formation of low-dimensional structures (such as nanoplatelets). With this approach, we also prepared NCs with two different sizes (edge lengths of 9.5 and 6.4 nm) to investigate the impact of the NC size on the optical properties. QAB-coated NCs were then prepared by performing a postsynthesis ligand exchange reaction on the former samples, as also reported in a previous work by our group.³⁹ The ligand exchange does not affect the overall morphology and structural properties of the NCs (see TEM images in Figure S7), and there is only a slight spectral blue-shift in the photoluminescence of ~10 meV (ascribed to mild surface etching²⁶), while the PLQY is increased.³⁹ Note that Cs oleate capped NCs are characterized by halide vacancies that are detrimental for the PLQY (which is typically <80% for these samples), whereas both mixed ligand capped NCs and QAB capped NCs have PLQYs of >90%, reaching 100% for the QAB capped ones in colloidal dispersions.^{32,38,39}

UV–vis absorption and PL spectra measured from the colloidal dispersions of Cs oleate capped NCs with different sizes are reported in panels a and b of Figure 4 (see Figure S7 for TEM images). The size uniformity of both samples is corroborated by the appearance of distinctive excitonic features in their optical absorption spectra (gray shaded spectra). Both samples manifest a single emission peak, with a narrow PL line width in the range of 72–73 meV. The PL peak position depends on quantum confinement, with a blue-shifted emission for the smaller NC sample (2.45 eV at RT) with respect to the larger one (2.41 eV at RT). The PL peak for both Cs oleate capped samples red-shifts with a decrease in temperature and becomes narrower in line width (Figure 4d,e,g,h). The PL amplitude is largest at low temperatures, manifesting a stretched exponential tail at its low-energy shoulder that can be ascribed to a broad band of defect states, probably due to halide vacancies. The red-shift with a decrease in temperature is significantly reduced for the smaller NC sample, which is in agreement with the results in ref 36. Studies on PbS NCs which show a qualitatively similar temperature-

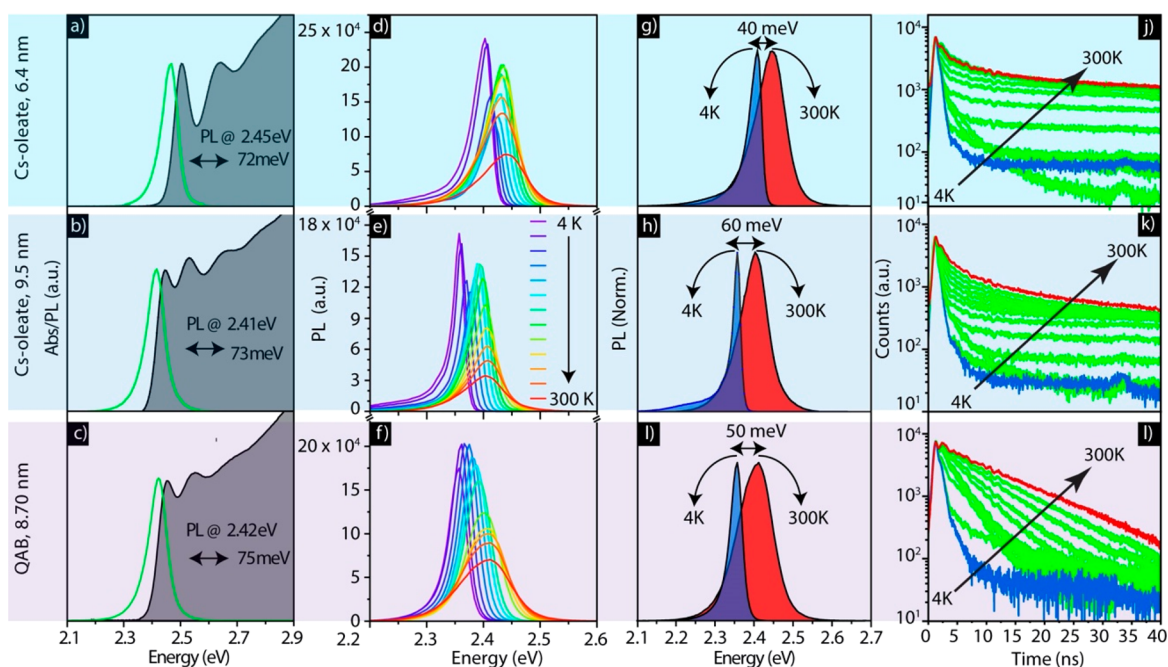


Figure 4. Optical features of CsPbBr₃ NCs with different sizes and surface coatings (either Cs oleate or QAB), as indicated for each row. Absorbance and PL spectra of Cs oleate capped NC with different sizes in a colloidal dispersion (a and b) and of QAB capped NCs obtained from a ligand exchange applied to the larger NC sample (c). (d–f) Temperature-dependent PL spectra recorded on films fabricated from these samples. (g–i) Comparison of spectra recorded from films of NCs at 4 and 300 K. PL intensities and line width vs temperature are reported in Figure S8. (j–l) Normalized PL decay traces collected at different temperatures from 4 to 300 K.

dependent band gap shift,⁴⁰ reveal the influence of the exciton binding energy, exciton–phonon coupling, and exciton fine structure at the band edge on this behavior.⁴¹ The PL decay traces are depicted in panels j and k of Figure 4 and show no NC size-related difference. For both NC sizes, a fast decay component develops and gains weight with a decrease in temperature, while the slower component decreases in weight in the cryogenic range.

The corresponding data for the QAB-coated NCs are reported in panels c, f, i, and l of Figure 4. Note that QAB ligands are proton-free, and therefore, NCs coated with these ligands are much more stable over time compared to the samples discussed above.^{29,39} Interestingly, the PL amplitude versus temperature and the PL decay traces are markedly different for the QAB-passivated NCs compared to the other samples. The PL decay traces show an almost monoexponential decay that also persists at lower temperatures, down to 170 K. The PL peak of the QAB-passivated sample at 4 K also has less tailing toward lower energies as compared to the other surface ligands, which indicates a lower density of trap states, thus confirming the more efficient passivation. These measurements demonstrate that the PL decay dynamics (and therefore the PL intensity) depend heavily on the surface passivation of the NC, while the PL energy and line width are defined by the NC size and choice of the monovalent (A) cation. From the decay dynamics of the samples with different ligands, we draw the following picture. The almost monoexponential decay at room temperature for mixed ligands and QAB passivation points to a single radiative decay channel and negligible nonradiative decay, which is corroborated by the high PL intensity. With a decrease in temperature, the PL intensity increases and the PL decay slope becomes steeper, indicating an increase in the radiative rate of that decay channel. With a further decrease in temperature, a faster decay component

emerges and the PL decay becomes biexponential. This can be rationalized by a deceleration of the dynamic ligand binding on the NC surface, which leads to less efficient passivation. This effect is balanced across an intermediate temperature range by the increasing rate of the radiative channel. At <50 K, the nonradiative decay takes over and the PL intensity drops significantly. For Cs oleate-passivated NCs, the PL decay is already biexponential at room temperature, which can be tentatively related to the presence of Br vacancies that induce nonradiative decay. This correlates well with the less efficient surface passivation of Cs oleate leading to lower PLQY.³⁸

The electronic structure, and therefore also the optical properties, are intimately related to the structure of the NC lattice, and temperature-dependent phase transitions from cubic to tetragonal to orthorhombic have been reported for lead halide perovskite films.^{42–46} Furthermore, it was recently demonstrated that structural defects have an impact on the phase transition in CsPbX₃ NCs at low temperatures.⁴⁷ To gain insight into the structural evolution of our NCs with temperature, and in particular to test if temperature-induced phase transitions occur in our NC samples, we carried out temperature-dependent X-ray diffraction (XRD) measurements on a mixed ligands and Cs oleate (see Figure S10 and Table S5) capped CsPbBr₃ NCs. Cs oleate capped NCs inherit significant halide defects, which is further reflected in their low PLQYs in the solution phase (<80%). Figure S9 shows the experimental patterns and relative Rietveld fits in the entire temperature range for mixed ligand capped CsPbBr₃ NCs. The acquired data were indexed to the diffraction pattern of the CsPbBr₃ orthorhombic phase (ICSD code 97851) and accordingly fitted in the entire temperature range (Figure S9). The variation with temperature of the *a*, *b*, and *c* lattice parameters and unit cell volume *V*, as extracted from the Rietveld fits, are displayed in Figure 5. No phase trans-

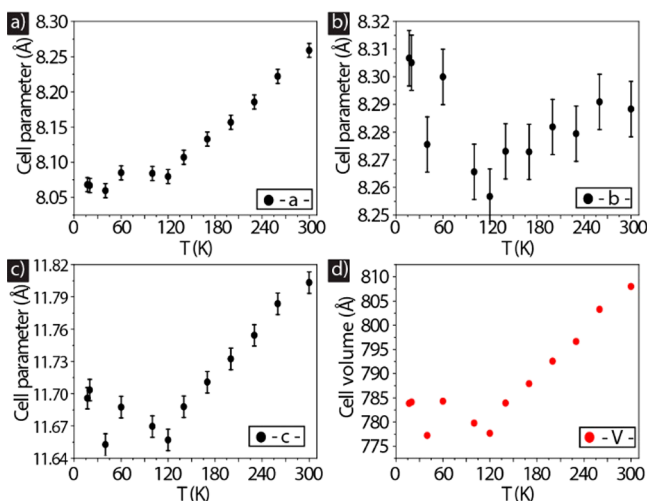


Figure 5. (a–d) Cell parameters (*a*, *b*, *c*, and *V*) obtained from the temperature-dependent XRD measurements of mixed ligand capped CsPbBr₃ NCs. The data yield a thermally induced expansion in the unit cell while retaining the orthorhombic phase.

formation was registered in the entire temperature range, in agreement with previous reports on CsPbX₃ NCs.^{15,48,49} When the NC films were cooled, Rietveld data analysis revealed a decrease in the *a* and *c* lattice parameters (note that *a* and *b* have almost the same value for this crystal structure; therefore, our analysis attributes most of the variation to one of the two parameters, in this case *a*), independent of the type of surface passivation. The relevant information resides in the volume of the unit cell that decreases with temperature. These changes in the unit cell were reversible when the NC film was heated back to 300 K. Overall, apart from a smooth decrease in cell parameters and cell volume, no phase transitions were observed in both mixed ligand and Cs oleate capped NCs.

In conclusion, our study of the photophysics of lead bromide perovskite NC films demonstrated that their low-temperature emission is defined by a single photoluminescence peak and that no temperature-induced phase transitions occur in these materials in the investigated temperature range. Therefore, the possible observation of multiple emission peaks at low temperatures^{16–20} should originate from different NC populations within the same sample. The PL peak energy and its temperature-induced shift are strongly related to the NC size, while the PL intensity and the recombination dynamics of the photoexcited carriers depend mostly on the surface functionalization. QAB ligands lead to improved PL stability and monoexponential PL decay over a larger temperature range among the three investigated types of surface passivation. The drop in PL intensity from 250 K to room temperature shows that the surface passivation of lead bromide perovskite NCs still needs to be improved toward a more stable ligand binding in the range exceeding room temperature. This is particularly important for the application of such materials in optoelectronic devices.

■ ASSOCIATED CONTENT

Supporting Information

The Supporting Information is available free of charge at <https://pubs.acs.org/doi/10.1021/acs.jpcllett.0c00266>.

Synthesis protocols, PL, PL decay traces and their multiexponential fitting parameters, TEM images for Cs

oleate and QAB capped CsPbBr₃ NCs, and XRD spectra recorded at different temperatures for mixed ligands and Cs oleate capped NCs (PDF)

■ AUTHOR INFORMATION

Corresponding Authors

Roman Krahne – Department of Nanochemistry, Istituto Italiano di Tecnologia, 16163 Genova, Italy; orcid.org/0000-0003-0066-7019; Email: roman.krahne@iit.it

Liberato Manna – Department of Nanochemistry, Istituto Italiano di Tecnologia, 16163 Genova, Italy; orcid.org/0000-0003-4386-7985; Email: liberato.manna@iit.it

Authors

Palvasha Ijaz – Department of Nanochemistry, Istituto Italiano di Tecnologia, 16163 Genova, Italy; Dipartimento di Chimica e Chimica Industriale, Università degli Studi di Genova, 16146 Genova, Italy

Muhammad Imran – Department of Nanochemistry, Istituto Italiano di Tecnologia, 16163 Genova, Italy; orcid.org/0000-0001-7091-6514

Márcio M. Soares – Brazilian Synchrotron Light Laboratory (LNLS), Brazilian Center for Research in Energy and Materials (CNPEM), Campinas, SP 13083-970, Brazil

Hélio C. N. Tolentino – Brazilian Synchrotron Light Laboratory (LNLS), Brazilian Center for Research in Energy and Materials (CNPEM), Campinas, SP 13083-970, Brazil

Beatriz Martín-García – Department of Nanochemistry and Graphene Laboratories, Istituto Italiano di Tecnologia, 16163 Genova, Italy; orcid.org/0000-0001-7065-856X

Cinzia Giannini – Istituto di Cristallografia-Consiglio Nazionale delle Ricerche (IC-CNR), I-70126 Bari, Italy; orcid.org/0000-0003-0983-2885

Iwan Moreels – Department of Nanochemistry, Istituto Italiano di Tecnologia, 16163 Genova, Italy; Department of Chemistry, Ghent University, 9000 Gent, Belgium

Complete contact information is available at: <https://pubs.acs.org/doi/10.1021/acs.jpcllett.0c00266>

Notes

The authors declare no competing financial interest.

■ ACKNOWLEDGMENTS

The research leading to these results has received funding from the European Union under Marie Skłodowska-Curie RISE Project COMPASS 691185. We thank Dr. Marti Ducastella and Dr. Dmitry Baranov for helpful discussions.

■ REFERENCES

- (1) Boles, M. A.; Ling, D.; Hyeon, T.; Talapin, D. V. The surface science of nanocrystals. *Nat. Mater.* **2016**, *15*, 141.
- (2) Chen, O.; Yang, Y.; Wang, T.; Wu, H.; Niu, C.; Yang, J.; Cao, Y. C. Surface-functionalization-dependent optical properties of II–VI semiconductor nanocrystals. *J. Am. Chem. Soc.* **2011**, *133*, 17504–17512.
- (3) Talapin, D. V.; Lee, J.-S.; Kovalenko, M. V.; Shevchenko, E. V. Prospects of colloidal nanocrystals for electronic and optoelectronic applications. *Chem. Rev.* **2010**, *110*, 389–458.
- (4) Shamsi, J.; Urban, A. S.; Imran, M.; De Trizio, L.; Manna, L. Metal halide perovskite nanocrystals: synthesis, post-synthesis modifications, and their optical properties. *Chem. Rev.* **2019**, *119*, 3296–3348.
- (5) Protesescu, L.; Yakunin, S.; Bodnarchuk, M. I.; Krieg, F.; Caputo, R.; Hendon, C. H.; Yang, R. X.; Walsh, A.; Kovalenko, M. V.

Nanocrystals of cesium lead halide perovskites (CsPbX_3 , $X = \text{Cl, Br, I}$): novel optoelectronic materials showing bright emission with wide color gamut. *Nano Lett.* **2015**, *15*, 3692–3696.

(6) Schmidt, L. C.; Pertegás, A.; González-Carrero, S.; Malinkiewicz, O.; Agouram, S.; Minguez Espallargas, G.; Bolink, H. J.; Galian, R. E.; Pérez-Prieto, J. Nontemplate synthesis of $\text{CH}_3\text{NH}_3\text{PbBr}_3$ perovskite nanoparticles. *J. Am. Chem. Soc.* **2014**, *136*, 850–853.

(7) Kovalenko, M. V.; Protesescu, L.; Bodnarchuk, M. I. Properties and potential optoelectronic applications of lead halide perovskite nanocrystals. *Science* **2017**, *358*, 745–750.

(8) Weidman, M. C.; Goodman, A. J.; Tisdale, W. A. Colloidal halide perovskite nanoplatelets: an exciting new class of semiconductor nanomaterials. *Chem. Mater.* **2017**, *29*, 5019–5030.

(9) Sutherland, B. R.; Sargent, E. H. Perovskite photonic sources. *Nat. Photonics* **2016**, *10*, 295.

(10) Quan, L. N.; Rand, B. P.; Friend, R. H.; Mhaisalkar, S. G.; Lee, T.-W.; Sargent, E. H. Perovskites for Next-Generation Optical Sources. *Chem. Rev.* **2019**, *119*, 7444–7477.

(11) Li, X.; Wu, Y.; Zhang, S.; Cai, B.; Gu, Y.; Song, J.; Zeng, H. CsPbX_3 quantum dots for lighting and displays: room-temperature synthesis, photoluminescence superiorities, underlying origins and white light-emitting diodes. *Adv. Funct. Mater.* **2016**, *26*, 2435–2445.

(12) Jing, P.; Zheng, J.; Ikezawa, M.; Liu, X.; Lv, S.; Kong, X.; Zhao, J.; Masumoto, Y. Temperature-dependent photoluminescence of CdSe-core CdS/CdZnS/ZnS-multishell quantum dots. *J. Phys. Chem. C* **2009**, *113*, 13545–13550.

(13) Zhao, Y.; Riemersma, C.; Pietra, F.; Koole, R.; de Mello Donegá, C.; Meijerink, A. High-temperature luminescence quenching of colloidal quantum dots. *ACS Nano* **2012**, *6*, 9058–9067.

(14) Diroll, B. T.; Nedelcu, G.; Kovalenko, M. V.; Schaller, R. D. High-Temperature Photoluminescence of CsPbX_3 ($X = \text{Cl, Br, I}$) Nanocrystals. *Adv. Funct. Mater.* **2017**, *27*, 1606750.

(15) Diroll, B. T.; Guo, P.; Schaller, R. D. Unique Optical Properties of Methylammonium Lead Iodide Nanocrystals Below the Bulk Tetragonal-Orthorhombic Phase Transition. *Nano Lett.* **2018**, *18*, 846–852.

(16) Li, J.; Yuan, X.; Jing, P.; Li, J.; Wei, M.; Hua, J.; Zhao, J.; Tian, L. Temperature-dependent photoluminescence of inorganic perovskite nanocrystal films. *RSC Adv.* **2016**, *6*, 78311–78316.

(17) Ramade, J.; et al. Fine structure of excitons and electron–hole exchange energy in polymorphic CsPbBr_3 single nanocrystals. *Nanoscale* **2018**, *10*, 6393–6401.

(18) Lee, S. M.; Moon, C. J.; Lim, H.; Lee, Y.; Choi, M. Y.; Bang, J. Temperature-dependent photoluminescence of cesium lead halide perovskite quantum dots: splitting of the photoluminescence peaks of CsPbBr_3 and $\text{CsPb}(\text{Br}/\text{I})_3$ quantum dots at low temperature. *J. Phys. Chem. C* **2017**, *121*, 26054–26062.

(19) Shinde, A.; Gahlaut, R.; Mahamuni, S. Low-temperature photoluminescence studies of CsPbBr_3 quantum dots. *J. Phys. Chem. C* **2017**, *121*, 14872–14878.

(20) Iaru, C. M.; Geuchies, J. J.; Koenraad, P. M.; Vanmaekelbergh, D. I.; Silov, A. Y. Strong carrier–phonon coupling in lead halide perovskite nanocrystals. *ACS Nano* **2017**, *11*, 11024–11030.

(21) De Roo, J.; Ibáñez, M.; Geiregat, P.; Nedelcu, G.; Walravens, W.; Maes, J.; Martins, J. C.; Van Driessche, I.; Kovalenko, M. V.; Hens, Z. Highly dynamic ligand binding and light absorption coefficient of cesium lead bromide perovskite nanocrystals. *ACS Nano* **2016**, *10*, 2071–2081.

(22) Smock, S. R.; Williams, T. J.; Brutchey, R. L. Quantifying the Thermodynamics of Ligand Binding to CsPbBr_3 Quantum Dots. *Angew. Chem.* **2018**, *130*, 11885–11889.

(23) Ravi, V. K.; Santra, P. K.; Joshi, N.; Chugh, J.; Singh, S. K.; Rensmo, H.; Ghosh, P.; Nag, A. Origin of the substitution mechanism for the binding of organic ligands on the surface of CsPbBr_3 perovskite nanocubes. *J. Phys. Chem. Lett.* **2017**, *8*, 4988–4994.

(24) Pan, A.; He, B.; Fan, X.; Liu, Z.; Urban, J. J.; Alivisatos, A. P.; He, L.; Liu, Y. Insight into the ligand-mediated synthesis of colloidal CsPbBr_3 perovskite nanocrystals: the role of organic acid, base, and cesium precursors. *ACS Nano* **2016**, *10*, 7943–7954.

(25) Yang, D.; Li, X.; Zeng, H. Surface chemistry of all inorganic halide perovskite nanocrystals: passivation mechanism and stability. *Adv. Mater. Interfaces* **2018**, *5*, 1701662.

(26) Koscher, B. A.; Swabeck, J. K.; Bronstein, N. D.; Alivisatos, A. P. Essentially trap-free CsPbBr_3 colloidal nanocrystals by postsynthetic thiocyanate surface treatment. *J. Am. Chem. Soc.* **2017**, *139*, 6566–6569.

(27) Wheeler, L. M.; Sanehira, E. M.; Marshall, A. R.; Schulz, P.; Suri, M.; Anderson, N. C.; Christians, J. A.; Nordlund, D.; Sokaras, D.; Kroll, T.; et al. Targeted Ligand-Exchange Chemistry on Cesium Lead Halide Perovskite Quantum Dots for High-Efficiency Photovoltaics. *J. Am. Chem. Soc.* **2018**, *140*, 10504–10513.

(28) Nenon, D. P.; Pressler, K.; Kang, J.; Koscher, B. A.; Olshansky, J. H.; Osowiecki, W. T.; Koc, M. A.; Wang, L.-W.; Alivisatos, A. P. Design Principles for Trap-Free CsPbX_3 Nanocrystals: Enumerating and Eliminating Surface Halide Vacancies with Softer Lewis Bases. *J. Am. Chem. Soc.* **2018**, *140*, 17760–17772.

(29) Bodnarchuk, M. I.; Boehme, S. C.; Ten Brinck, S.; Bernasconi, C.; Shynkarenko, Y.; Krieg, F.; Widmer, R.; Aeschlimann, B.; Günther, D.; Kovalenko, M. V.; et al. Rationalizing and controlling the surface structure and electronic passivation of cesium lead halide nanocrystals. *ACS Energy Lett.* **2019**, *4*, 63–74.

(30) Leung, K.; Whaley, K. B. Surface relaxation in CdSe nanocrystals. *J. Chem. Phys.* **1999**, *110*, 11012–11022.

(31) Wuister, S. F.; van Houselt, A.; de Mello Donegá, C.; Vanmaekelbergh, D.; Meijerink, A. Temperature anti-quenching of the luminescence from capped CdSe quantum dots. *Angew. Chem., Int. Ed.* **2004**, *43*, 3029–3033.

(32) Imran, M.; Caligiuri, V.; Wang, M.; Goldoni, L.; Prato, M.; Krahn, R.; De Trizio, L.; Manna, L. Benzoyl halides as alternative precursors for the colloidal synthesis of lead-based halide perovskite nanocrystals. *J. Am. Chem. Soc.* **2018**, *140*, 2656–2664.

(33) Zhang, F.; Zhong, H.; Chen, C.; Wu, X.-g.; Hu, X.; Huang, H.; Han, J.; Zou, B.; Dong, Y. Brightly luminescent and color-tunable colloidal $\text{CH}_3\text{NH}_3\text{PbX}_3$ ($X = \text{Br, I, Cl}$) quantum dots: potential alternatives for display technology. *ACS Nano* **2015**, *9*, 4533–4542.

(34) Dar, M. I.; Jacopin, G.; Meloni, S.; Mattoni, A.; Arora, N.; Boziki, A.; Zakeeruddin, S. M.; Rothlisberger, U.; Grätzel, M. Origin of unusual bandgap shift and dual emission in organic-inorganic lead halide perovskites. *Sci. Adv.* **2016**, *2*, No. e1601156.

(35) D'innocenzo, V.; Grancini, G.; Alcocer, M. J.; Kandada, A. R. S.; Stranks, S. D.; Lee, M. M.; Lanzani, G.; Snaith, H. J.; Petrozza, A. Excitons versus free charges in organo-lead tri-halide perovskites. *Nat. Commun.* **2014**, *5*, 3586.

(36) Naghadeh, S. B.; Sarang, S.; Brewer, A.; Allen, A. L.; Chiu, Y.-H.; Hsu, Y.-J.; Wu, J.-Y.; Ghosh, S.; Zhang, J. Z. Size and temperature dependence of photoluminescence of hybrid perovskite nanocrystals. *J. Chem. Phys.* **2019**, *151*, 154705.

(37) Woo, H. C.; Choi, J. W.; Shin, J.; Chin, S.-H.; Ann, M. H.; Lee, C.-L. Temperature-Dependent Photoluminescence of $\text{CH}_3\text{NH}_3\text{PbBr}_3$ Perovskite quantum dots and bulk counterparts. *J. Phys. Chem. Lett.* **2018**, *9*, 4066–4074.

(38) Imran, M.; Ijaz, P.; Baranov, D.; Goldoni, L.; Petralanda, U.; Akkerman, Q.; Abdelhady, A. L.; Prato, M.; Bianchini, P.; Infante, I.; et al. Shape-Pure, Nearly monodispersed CsPbBr_3 nanocubes prepared using secondary aliphatic amines. *Nano Lett.* **2018**, *18*, 7822–7831.

(39) Imran, M.; Ijaz, P.; Goldoni, L.; Maggioni, D.; Petralanda, U.; Prato, M.; Almeida, G.; Infante, I.; Manna, L. Simultaneous cationic and anionic ligand exchange for colloidally stable CsPbBr_3 nanocrystals. *ACS Energy Lett.* **2019**, *4*, 819–824.

(40) Olkhovets, A.; Hsu, R. C.; Lipovskii, A.; Wise, F. W. Size-dependent temperature variation of the energy gap in lead-salt quantum dots. *Phys. Rev. Lett.* **1998**, *81*, 3539–3542.

(41) Hu, Z.; Kim, Y.; Krishnamurthy, S.; Avdeev, I. D.; Nestoklon, M. O.; Singh, A.; Malko, A. V.; Goupalov, S. V.; Hollingsworth, J. A.; Htoon, H. Intrinsic exciton photophysics of PbS quantum dots revealed by low-temperature single nanocrystal spectroscopy. *Nano Lett.* **2019**, *19*, 8519–8525.

(42) Guo, Y.; Yaffe, O.; Paley, D. W.; Beecher, A. N.; Hull, T. D.; Szpak, G.; Owen, J. S.; Brus, L. E.; Pimenta, M. A. Interplay between organic cations and inorganic framework and incommensurability in hybrid lead-halide perovskite $\text{CH}_3\text{NH}_3\text{PbBr}_3$. *Phys. Rev. Mater.* **2017**, *1*, 042401.

(43) Chen, T.; et al. Origin of long lifetime of band-edge charge carriers in organic–inorganic lead iodide perovskites. *Proc. Natl. Acad. Sci. U. S. A.* **2017**, *114*, 7519.

(44) Wu, K.; Bera, A.; Ma, C.; Du, Y.; Yang, Y.; Li, L.; Wu, T. Temperature-dependent excitonic photoluminescence of hybrid organometal halide perovskite films. *Phys. Chem. Chem. Phys.* **2014**, *16*, 22476–22481.

(45) Fang, H.-H.; Wang, F.; Adjokatse, S.; Zhao, N.; Even, J.; Antonietta Loi, M. Photoexcitation dynamics in solution-processed formamidinium lead iodide perovskite thin films for solar cell applications. *Light: Sci. Appl.* **2016**, *5*, e16056–e16056.

(46) Wright, A. D.; Verdi, C.; Milot, R. L.; Eperon, G. E.; Pérez-Osorio, M. A.; Snaith, H. J.; Giustino, F.; Johnston, M. B.; Herz, L. M. Electron–phonon coupling in hybrid lead halide perovskites. *Nat. Commun.* **2016**, *7*, 11755.

(47) Ahmad, A.; Mukherjee, P.; Mandal, D.; Senapati, S.; Khan, M. I.; Kumar, R.; Sastry, M. Enzyme mediated extracellular synthesis of CdS nanoparticles by the fungus, *Fusarium oxysporum*. *J. Am. Chem. Soc.* **2002**, *124*, 12108–12109.

(48) Yang, R. X.; Skelton, J. M.; Da Silva, E. L.; Frost, J. M.; Walsh, A. Spontaneous octahedral tilting in the cubic inorganic cesium halide perovskites CsSnX_3 and CsPbX_3 ($X = \text{F}, \text{Cl}, \text{Br}, \text{I}$). *J. Phys. Chem. Lett.* **2017**, *8*, 4720–4726.

(49) Cottingham, P.; Brutchey, R. L. Depressed phase transitions and thermally persistent local distortions in CsPbBr_3 quantum dots. *Chem. Mater.* **2018**, *30*, 6711–6716.